Springer

KSME

Journal of Mechanical Science and Technology 26 (12) (2012) 3751~3759
www.springerlink.com/content/1738-494x
DOI 10.1007/s12206-012-1001-7

Capillary-driven micro flows for the underfill process in microelectronics packaging †

Young Bae Kim[1] and Jaeyong Sung[2,*]

[1]*Graduate School of Energy and Environment, Seoul National University of Science and Technology, Seoul 139-743, Korea*
[2]*Department of Mechanical and Automotive Engineering, Seoul National University of Science and Technology, Seoul 139-743, Korea*

(Manuscript Received May 22, 2012; Revised June 6, 2012; Accepted June 18, 2012)

Abstract

Capillary-driven micro flow allows liquid transport by interfacial force without external pressure or momentum. Theoretical and experimental studies have been conducted to predict the movement of the flow meniscus in the application of capillary underfill flows. In a flip chip package, two-dimensional motions of flow front through solder bumps can result in unwanted air void formation because the meniscus and the arrangement of the solid surface affect the interface dynamics. This study introduces analytical models of filling time and discusses their verification and limitations. Recent developments in underfill flow visualization are also presented to analyze flow phenomena, including the racing effect and void formation.

Keywords: Capillary underfill flow; Filling time model; Flip chip package; Flow visualization; Void formation

1. Introduction

Liquid penetrates into a narrow gap by capillary action at the gas–liquid interface. This process is called microcapillary flow and has practical importance in a wide range of technologies such as the flow through porous materials in micro heat pipes and micro coolers as well as underfilling in flip chip packaging. The fundamental physics of microcapillary flows has long been examined, specifically, the movement of the flow meniscus through a capillary tube or channel [1-3].

Meanwhile, flip chip technology is widely used to package high-performance devices and satisfy the need for high interconnection density [4]. Fig. 1(a) shows the comparison of the internal structures of flip chip and wire bond packages. The flip chip indicates that the patterned face of a chip with solder bumps is turned over to interconnect directly to a substrate with solder balls. In a wire bond package, long conductive wires are connected between a chip and a substrate. The short interconnection in the flip chip technology is more advantageous than the long wire connection for manufacturing thinner and smaller integrated circuit systems and improving electrical performance. The solder balls in the packaged chip are welded to electric pads on a printed circuit board. However, in flip chip packages, underfill epoxy should be filled into the gap between a chip and a substrate to prevent cracks on the solder bump and electrical failure resulting from thermal fatigue. A large difference in the thermal expansion coefficient (CTE) between the silicon chip and the organic substrate may cause significant thermal stresses on the interconnections during thermal cycling [5]. Thus, the underfill epoxy relaxes the stresses by the CTE mismatch, as well as reduces the impact and deflection of the substrate. The filling method can be classified into capillary underfill or no-flow underfill. This study focuses on the capillary underfill process, as shown in Fig. 1(b). In this process, the underfill epoxy is dispensed along the

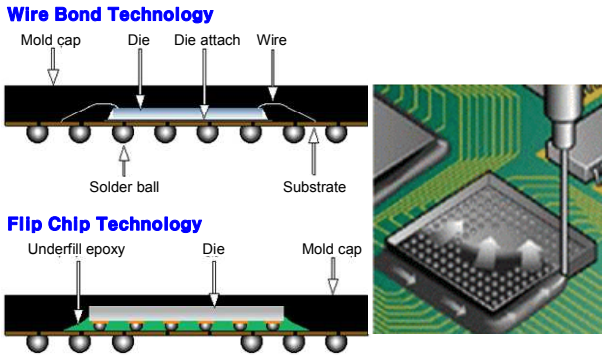

Fig. 1. (a) Internal structures of wire bond and flip chip packages; (b) capillary underfill process to improve reliability of interconnection system.

*Corresponding author. Tel.: +82 2 970 6398, Fax.: +82 2 949 1458
E-mail address: jysung@seoultech.ac.kr
† This paper was presented at the Workshop honoring professor Jung Yul Yoo on his Official Retirement, Seoul, Korea, March 2012.

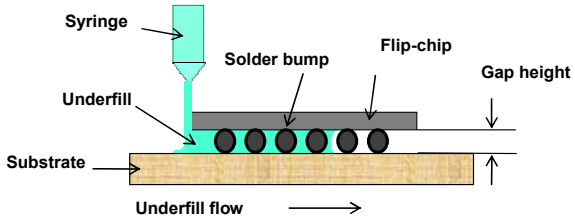

Fig. 2. Schematic of the capillary underfill process.

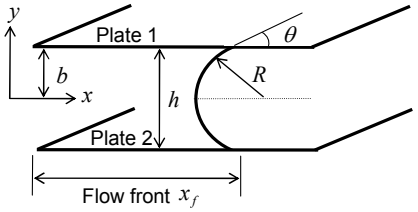

Fig. 3. Capillary flow through two parallel plates.

periphery of one or two sides of the chip, allowing the capillary action to draw the liquid into the microcavity [6]. Given that the filling process is based on the capillary action, a longer filling time is required for a larger chip size and a higher bump density. Air voids may occur when the underfill material is not uniformly distributed, which results in a significant reliability problem in microelectronic packaging.

In this survey, capillary-driven micro flows in the underfill process are introduced. For a given solder bump pattern and underfill epoxy, estimating the filling time is one of the main problems in the underfill process design. Several filling time models based on the theory of microcapillary flow have been developed with solder bump resistance, dynamic contact angle, and non-Newtonian and temperature-dependent fluid properties considered. The analytical models of filling time have been verified experimentally and numerically. The second problem is the physical flow phenomenon in the capillary underfill flow. Air void formation by the racing effect is one of the important practical issues to consider. Void formation is mainly related to the dynamic interaction between the flow meniscus and the solder bumps. Recent success in microscale flow visualization can address this unwanted filling process.

2. Filling time models

Fig. 2 presents a diagram of the underfill flow process. The underfill epoxy is dispensed at the edge of a flip chip specimen. The liquid is then filled into the gap between a substrate and a flip chip by capillary action; the typical gap height is about 50 μm. Before the liquid is dispensed, it is heated up to 90ºC to increase the flow by viscosity reduction. During heating, the temperature is maintained under the curing temperature; above said temperature, the liquid hardens immediately. At temperatures lower than the curing temperature, the liquid can harden if exposed to the atmosphere, which suggests a limitation for the filling time to complete the underfill process. Thus, filling time estimation is one of the major considerations in the underfill process design. Several filling time models have been suggested over the past decades.

2.1 Flow between two parallel plates

A simple filling time model can be derived by assuming that the liquid is filled through a narrow gap between two parallel plates without a solder bump, as shown in Fig. 3. For a Newtonian viscous liquid, if the flow is laminar and incompressible, and the governing equation for the unsteady flow $u(y, t)$ can be expressed as follows:

$$\rho\frac{\partial u}{\partial t}=-\frac{\partial p}{\partial x}+\mu\frac{\partial^2 u}{\partial y^2} \tag{1}$$

where μ is the fluid viscosity and ρ is the density. From the Laplace–Young equation, the driving capillary force at the meniscus is $\Delta p=2\sigma\cos\theta/h$, where σ is the surface tension coefficient, θ is the contact angle, and $h = 2b$ is the gap height. Given that Eq. (1) cannot be solved analytically, the velocity is decomposed into steady and unsteady terms as $u(y,t)=\bar{u}(y)+u'(y,t)$. By letting $\bar{u}$ and u' stratify, the following are obtained:

$$0=-\frac{dp}{dx}+\mu\frac{\partial^2\bar{u}}{\partial y^2} \tag{2}$$

$$\rho\frac{\partial u'}{\partial t}=\mu\frac{\partial^2 u'}{\partial y^2}. \tag{3}$$

The solution of the steady component is the well known, fully developed laminar velocity profile, and the solution of the unsteady component can be obtained by the separation of variables proposed by Arpaci [7].

$$\bar{u}=-\frac{dp/dx}{2\mu}(b^2-y^2)\quad\text{and} \tag{4}$$

$$u'=\sum_{n=0}^{\infty}a_n\exp(-\lambda_n^2\nu t)\cos\lambda_n y \tag{5}$$

where $\lambda_n b=\dfrac{(2n+1)\pi}{2}$, $n=0, 1, 2, \cdots$

$$a_n=-2\frac{(-dp/dx)}{\mu}\frac{(-1)^n b^2}{(\lambda_n b)^3}.$$

The pressure gradient inside the channel is assumed as linear; i.e., $-dp/dx=\Delta p/x_f$, where x_f is the location of the flow front. The speed of the flow front is equal to the mean velocity u_m, which can be evaluated by integrating the velocity profile across the channel cross-section.

$$u_m=\frac{dx_f}{dt}=\frac{\Delta p b^2}{x_f\mu}\left[\frac{1}{3}-2\sum_{n=0}^{\infty}\frac{1}{(\lambda_n b)^4}\exp(-\lambda_n^2\nu t)\right] \tag{6}$$

Integration of the above equation with respect to time [0, t_f] obtains the following:

$$x_f^2 = \frac{2\Delta p b^2}{\mu}\left[\frac{1}{3}t_f - 2\sum_{n=0}^{\infty}\frac{1}{(\lambda_n b)^4}\frac{1}{\lambda_n^2 \nu}\left(1-\exp(-\lambda_n^2 \nu t_f)\right)\right] \approx \frac{2\Delta p b^2}{\mu}\left(\frac{1}{3}t_f - \frac{32h^2}{\pi^6 \nu}\right) \quad (7)$$

where only the first term (n = 0) in the series expansion is considered because it decreases quickly with the increase in n. To obtain an explicit formula for time t_f, the exponential term can also be neglected except for the time less than 0.002 s despite the unsatisfied initial condition (x_f = 0 at t_f = 0). By substituting the capillary pressure Δp into Eq. (7), the final equation for the filling time can be obtained as

$$t_f = \frac{6\mu x_f^{\,2}}{\Delta p h^2} + \frac{96h^2}{\pi^6 \nu} = \frac{3\mu x_f^{\,2}}{h\sigma\cos\theta} + \frac{96h^2}{\pi^6 \nu}. \quad (8)$$

The first term in the right-hand side of Eq. (8) results from the steady velocity component and is the same as that in the Washburn model [1]. The second term is the maximum contribution of the unsteady velocity component, which is related to the gap height h and the kinematic viscosity ν of the fluid. For the narrower gap height and the more viscous liquid, the unsteady flow has less effect on the filling time. With the typical gap height of 50 μm and glycerin as a working fluid, the filling time caused by the unsteady flow is about 0.2 μs. For the viscosity of water, the filling time is 250 μs, which is negligible, considering that the total filling time in real applications is more than 10 s.

2.2 Influence of solder bump resistance

The diameter and pitch of the solder bump in flip chips have decreased significantly because of the demand for smaller and thinner electronic devices. Consequently, a chip with a higher density of solder bump is required. Thus, predicting the filling time based on the Washburn model is not satisfactory because it does not consider the existence of the solder bump. Several experimental studies [8, 9] reported that the actual filling time was longer than the time estimated by the Washburn model. To consider the influence of solder bump resistance on the capillary underfill flow, Wan et al. [10] suggested an advanced model (referred to as the Wan model) for a rectangular array of the solder bump pattern, as shown in Fig. 4(a). In the figure, L is the bump pitch, W is the clearance between two adjacent solder bumps, and d is the bump diameter. The underfill flow passing through the solder bump array is approximated as a combination of a set of one-dimensional channel flows with a variable cross-section, as illustrated in Fig. 4(b). Despite the two-dimensional velocity field, only the streamwise component averaged over the cross-section is considered. In this geometry, the driving pressure of

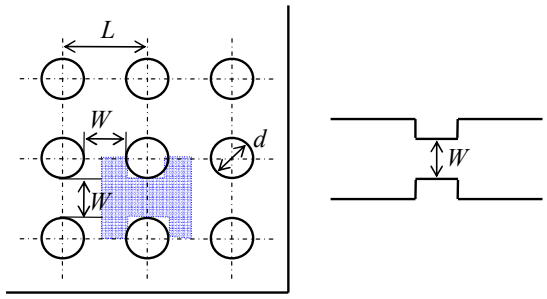

Fig. 4. Flip chip package pattern: (a) a rectangular array of the solder bump pattern; (b) an approximate flow passage through a solder bump array.

the capillary force is reduced by the pressure loss because of the variation of the cross-section, which can be calculated from the virtual work principle [11]. The final equation of the driving pressure is written as follows:

$$\Delta p = \Delta p_{capillary} - \Delta p_{bump} = 2\sigma\cos\theta\left(\frac{1}{W}+\frac{1}{h}\right) - \frac{2d\sigma\cos\theta}{W(W+d)} = \frac{2\sigma\cos\theta(W^2+hW+dW-dh)}{hW(W+d)}. \quad (9)$$

This equation is reproduced to the Laplace–Young equation without a solder bump if W becomes infinite. The resultant driving pressure in this model is constant if the geometry and fluid properties are fixed. By substituting Eq. (9) for the driving pressure into Eq. (8), the filling time can be evaluated.

2.3 Time-dependent dynamic contact angle

In both Washburn and Wan models, the contact angle is assumed constant as an equilibrium contact angle. In reality, at the early stage of the underfill process, the contact angle is nearly 90º because the meniscus of the liquid dispensed at the edge of the channel forms a right angle in the stream direction. With time, the contact angle develops to its equilibrium angle. The use of the constant contact angle suggests that the development of an equilibrium contact angle is too fast that the developing region is neglected. However, studies demonstrated that the time-dependent dynamic contact angle had to be considered [12, 13].

For the dynamic contact angle, Newman [14] proposed the equation $\cos\theta(t) = \cos\theta_s(1-ae^{-ct})$, where the contact angle decreases exponentially with time, as shown in Fig. 5. In the figure, θ_s is the static or equilibrium contact angle, and θ_0 is the initial contact angle. $a = 1-\cos\theta_0/\cos\theta_s$ and $c = \sigma/(\mu M)$ are the coefficients, where M is a constant that depends on the solid surface. Given that the contact angle is a function of time, the driving pressure also changes with time. Thus, the integration of Eq. (6) by neglecting the unsteady flow component results in the following formula for the filling time:

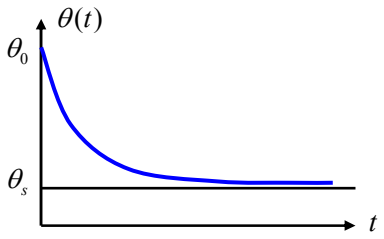

Fig. 5. Time-dependent dynamic contact angle proposed by Newman [14].

$$t_f = \frac{6\mu x_f^2}{\Delta p h^2} + \frac{a}{c}\left(1 - e^{-ct_f}\right). \tag{10}$$

This equation is a nonlinear function of the filling time, which requires an iterative solution. To calculate the driving pressure in the above equation, either the Washburn or the Wan model can be used.

2.4 Non-Newtonian and temperature-dependent fluids

The properties of the underfill materials are additional key issues in underfill flow modeling. Two aspects of material properties have to be considered in the actual applications. One is the rheological characteristic, and the other is the temperature dependency of the properties. The underfill materials are generally known as non-Newtonian fluids. The most widely employed formula as a constitutive equation of viscosity is the power-law model [15, 16], in which the effective viscosity is given by $\eta = m\dot{\gamma}^{n-1}$. In this model, the viscosity varies with the shear rate $\dot{\gamma}$, and the parameters m and n are determined experimentally. For a Newtonian fluid, m = μ and n = 1. If $n > 1$, the fluid is called shear thickening; if $n < 1$, the fluid is called shear thinning. The governing Eq. (1) for a non-Newtonian fluid by neglecting the unsteady velocity component can be rewritten as

$$\frac{d}{dy}\left(\eta \frac{du}{dy}\right) = -\frac{dp}{dx}. \tag{11}$$

By integrating the aforementioned equation, the velocity profile inside the channel can be obtained as

$$u(y) = \frac{n}{n+1}\left(\frac{-dp/dx}{m}\right)^{\frac{1}{n}}\left(b^{\frac{n+1}{n}} - y^{\frac{n+1}{n}}\right). \tag{12}$$

Using the same procedure conducted on the Newtonian fluid explained previously, the final equations for the flow front and filling time can be derived as

$$x_f = \frac{h}{2}\left(\frac{\Delta p}{m}\right)^{\frac{1}{n+1}}\left(\frac{n+1}{2n+1} t_f\right)^{\frac{n}{n+1}} \tag{13}$$

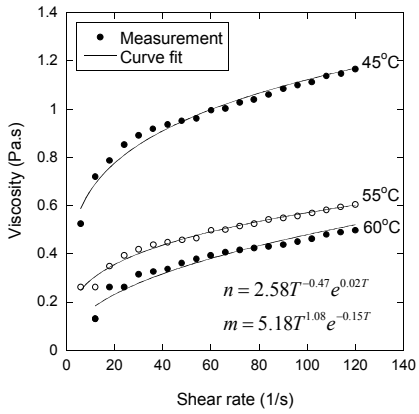

(a)

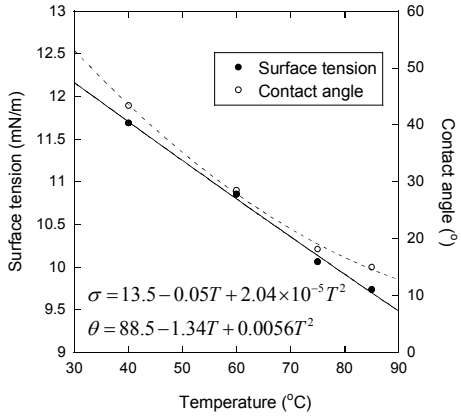

(b)

Fig. 6. Temperature-dependent properties of an underfill material FP4530: (a) viscosity; (b) surface tension and contact angle (Wan [17]).

$$t_f = \frac{n+1}{2n+1}\left(\frac{\Delta p}{m}\right)^{\frac{1}{n}}\left(\frac{2x_f}{h}\right)^{\frac{n+1}{n}} \tag{14}$$

where the driving pressure can be either the capillary pressure or the net pressure with bump resistance considered, as suggested by the Washburn and Wan models, respectively.

To calculate the filling time in Eq. (14), the properties of underfill materials, such as density, surface tension, and contact angle as well as the power-law indices of viscosity, must be determined. Except for density, these properties of typical underfill materials are sensitive to temperature variations. Fig. 6 shows the temperature-dependent properties of an underfill material FP4530 (Dexter Corp., USA) [17]. In general, the underfill material is stored below -40ºC to prevent hardening. Above room temperature, its viscosity becomes sufficiently low to make a capillary underfill flow. The viscosity illustrated in Fig. 6(a) changes with the shear rate and is adequately fitted to the power-law constitutive equation for 45, 55, and 60ºC. This material has a shear-thinning behavior in the processing temperature range. The dependence of m and n on temperature is shown in Fig. 6(a). In the figure, m decreases

with temperature, which contributes to the decrease in viscosity; whereas *n* increases with temperature, which enhances the shear thinning behavior. The surface tension and equilibrium contact angle are also measured under the variation of temperature, as shown in Fig. 6(b). Both properties decrease with temperature, but the decreasing rate of the contact angle is more significant than that of the surface tension. The contact angle is also dependent on the surface materials of the chip and substrate [18].

2.5 Influence of capillary pressure on solder bump surface

Young [19, 20] derived a different filling time model (the Young model) by considering viscous resistance and variable capillary pressure on the solder bump according to the location of the flow meniscus. The flow domain is regarded as a porous space with an array of circular cylinder banks and confined by two parallel plates. The viscous drag consists of the resistance values by both the channel walls and the solder bumps. For a given pressure gradient, the mean velocity between the parallel plates can be obtained by integrating Eq. (4) over the channel cross-section as follows:

$$u_m = -\frac{h^2}{12\mu}\frac{dp}{dx}. \tag{15}$$

If the solder bumps are considered as parallel cylinders, the flow between the circular cylinders can be expressed as [21]

$$u_m = -\frac{4d^2}{9\sqrt{2}\pi\mu}\left(\frac{L-d}{d}\right)^{5/2}\frac{dp}{dx}. \tag{16}$$

By combining the flow resistances in Eqs. (15) and (16), the mean velocity for a given pressure gradient can be written as:

$$u_m = -\frac{k}{\mu}\frac{dp}{dx}, \quad k = \left[\frac{9\sqrt{2}\pi}{4d^2}\left(\frac{d}{L-d}\right)^{5/2} + \frac{12}{h^2}\right]^{-1}, \tag{17}$$

where k is the permeability, and L is the bump pitch.

With the meniscus located at the position x_f as shown in Fig. 7, the mean velocity varies depending on the position x due because of the change in the cross-sectional area $A(x)$ to satisfy mass conservation.

$$u_m(x) = u_m(x_f)\frac{A(x_f)}{A(x)} \tag{18}$$

The speed of the flow front is equal to the mean velocity at the meniscus, i.e., $u_m(x_f) = dx_f/dt$. Assuming that the pressure gradient is linear and integrating Eq. (17) from the entrance to the meniscus position, the following relationship between the meniscus wetting distance and the capillary pressure can be derived in terms of the accumulated viscous resistance $R(x_f)$ along the flow path:

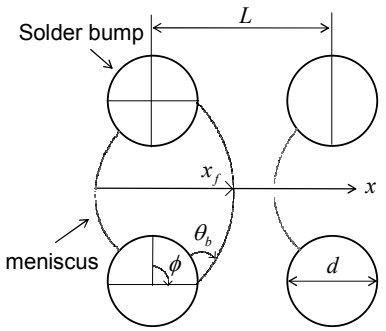

Fig. 7. A flow model considering the variable capillary pressure on the solder bump according to the location of the flow meniscus.

$$\mu A(x_f)R(x_f)\frac{dx_f}{dt} = \Delta p\ , \quad R(x_f) = \int_0^{x_f}\frac{dx}{kA(x)}. \tag{19}$$

The final meniscus wetting distance can be obtained by integrating dx_f/dt into Eq. (19). In this equation, the cross-sectional area, viscous resistance, and capillary pressure differ whether or not the position is in the region of the solder bump. In the bump region, they are evaluated from the following formulas:

$$A(x) = L - d\cos\phi \tag{20}$$

$$R(x) = \int_{-\pi/2}^{\phi}\frac{d\cos\phi d\phi}{2hk(L-d\cos\phi)} + R^{i-1} \tag{21}$$

$$\Delta p = \frac{2\sigma_b\cos(\theta_b+\phi)}{L-d\cos\phi} + \frac{2\sigma\cos\theta}{h}. \tag{22}$$

When the meniscus is located outside the bump region, the following formulas are used:

$$A(x) = Lh \tag{23}$$

$$R(x) = \int_{-\pi/2}^{\pi/2}\frac{d\cos\phi d\phi}{2hk(L-d\cos\phi)} + \frac{12}{h^3L}(x_f^i - d) + R^{i-1} \tag{24}$$

$$\Delta p = \frac{2\sigma\cos\theta}{h} \tag{25}$$

where ϕ is the directional body angle formed by the contact line on the solder bump, and σ_b and θ_b are the surface tension and contact angle on the bump surface, respectively. Superscripts *i*-1 and *i* are the previous and current layers of the bump array, respectively. Thus, R^{i-1} denotes the accumulated viscous resistance until the previous layer. In the bump region, two capillary pressures are involved in the underfill process, as shown in Eq. (22). One is the capillary pressure caused by the surface tension between solder bumps, which may become significant as the bump pitch becomes smaller; the other is the capillary pressure exerted by the surface tension between the parallel plates, which is commonly considered in the Washburn and Wan models.

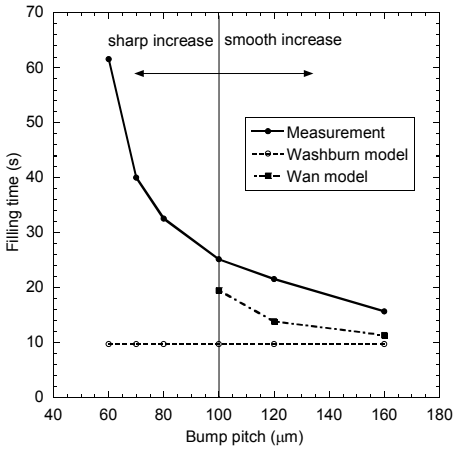

Fig. 8. Comparison of the measured filling time with the estimated filling time by the analytical models (Kim et al. [24]).

2.6 Experimental verification of filling time models

In numerous studies, the filling time models have been verified experimentally. The results showed that the Washburn model could be inaccurate because of the flow resistance of solder bumps if the clearance between the bumps is comparable to the gap height [22]. For a flip chip package with a relatively high bump density (a bump diameter of 100 μm, a bump pitch of 250 μm, a and gap height of 50 μm), the Wan model, including both the solder bump resistance and the rheological behavior of the non-Newtonian fluid, can provide a closer estimate of the filling time [23]. With regard to the dynamic contact angle, Han and Wang [22] applied the Newman equation for the first time in estimating the filling time in a flip chip package. The model using the dynamic contact angle was superior to the model using the static contact angle. However, the estimated filling time and the experimental results did not match. The most probable reason is that the Newman equation developed for the flow between the two parallel plates did not include the effect of solder bumps on the underfill flow, especially in a high bump density.

Kim et al. [24] compared the filling time estimated by the Washburn and Wan analytical models with the experimental data, including the case when the clearance between the bumps is less than the bump diameter or gap height. Fig. 8 shows the comparison of filling times for various bump pitches. Both the bump diameter and the gap height are 50 μm, and a Newtonian fluid is underfilled. The filling times in both analytical models are shorter than that in the experiment, especially in small bump pitches. The filling time increases sharply as the bump pitch becomes smaller than twice the bump diameter. However, in the Wan model, the filling time in an extremely high bump density cannot be calculated because the capillary pressure in Eq. (9) becomes negative. Furthermore, Lee et al. [25] measured the detailed behavior of the flow front movement in one pitch of the solder bump by using a microscope. The experimental data indicate that the flow front movement is not monotonic but rather, is dependent on the location of the flow front. When the flow front passes through the solder bump, its movement becomes fast because of the additional capillary action by the solder bump surface, which can be well estimated by the Young model. However, the flow front movement becomes slower during the detachment from the solder bump because the solder bump prevents it from detaching. Consequently, a breakdown of equilibrium in the contact angle occurs because of the dynamic interaction with the surface of the solder bump. The variation in the contact angle is in phase with the variation in the flow front speed [25]. This phenomenon has not been considered in previous analytical models.

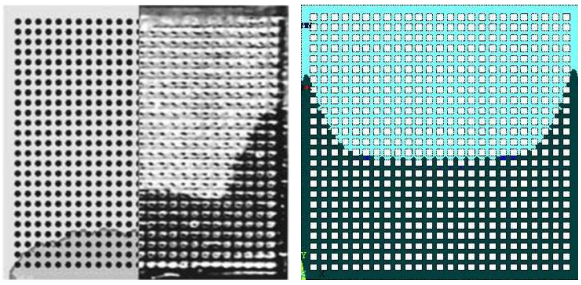

(a) (b)

Fig. 9. Flow visualization of the racing effect: (a) omparison of simulated flow front (left) and measured flow front (right) by Nguyen et al. [8]; (b) more advanced simulation for flow front by Wan et al. [27].

3. Physical phenomena in capillary underfill flows

3.1 Racing effect and void formation

The analytical models only consider the parallel movement of the flow front with time. However, the top view of the two-dimensional flow shows that the flow front is not always uniform, as shown in Fig. 9. Experimental results indicated that a faster flow develops along the edge [26]. Nguyen et al. [8] referred to this phenomenon as the "racing effect", which may cause air void formation at the center of the chip. If the air void is formed inside the chip, high stress is concentrated in the void region, which greatly reduces the reliability of the flip chip package. Thus, the design of the underfill flow without void formation is a critical issue in the industrial field. Numerical simulations have been performed to estimate void formation. Fig. 9(a) shows the comparison of the simulated flow front and the measured flow front by Nguyen et al. [8]. The right side corresponds to the measured flow front with a transparent quartz die ($6.7 \times 6.7 \times 0.6$ mm thick). The bump diameter is 168 μm, and the bump pitch is 262 μm. The flow simulation was performed using the commercial software (PLICE-CAD); however, the simulation result did not match the measured result. Wan et al. [27] recently simulated the same flow with the ANSYS software based on the volume-of-fluid method. Their result successfully estimated the faster flow along the edge region, as shown in Fig. 9(b). The main reason for this success is that a solid frame is set around the sides of the flip chip, and the edge width (the distance between

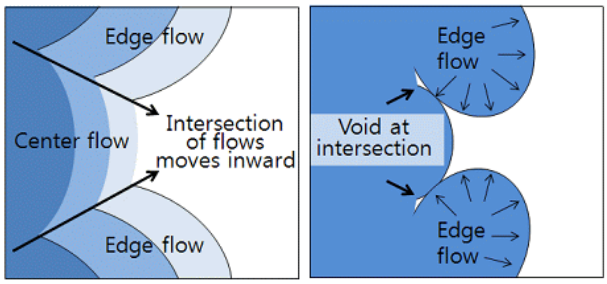

Fig. 10. Merging of the flow fronts and void formation by the racing effect: (a) development of flow front by fast edge and slow center flows; (b) void formation at the intersection of the flow fronts.

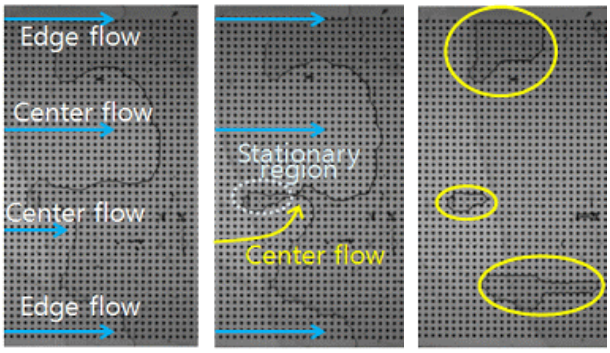

Fig. 11. Flow visualization of void formation by the racing effect with laps of time: (a) non-uniform flow fronts with different velocities at the early stage; (b) flow fronts encountered at the stationary regions; (c) irremovable voids after the filling process.

the outside solder bump and the edge) is adequately controlled. As the bump density increases, the effect of the edge width becomes significant. Thus, to obtain a uniform flow front distribution and prevent the formation of air voids, a sufficiently small edge is required. Despite the partial success in the estimation of the faster edge flow, the detailed shape of the flow front does not match the measured results because their simulation is two-dimensional. To overcome this limitation, Hashimoto et al. [28] conducted a numerical simulation of three-dimensional underfill flows using the level set method for gas–liquid interface and the continuum surface force model for surface tension. The results were compared with the available experimental data, and the void formation mechanism was observed.

Fig. 10 depicts air void formation by the racing effect. Given a slow center flow, the fronts of the fast edge flow in both sides are inclined toward the center. The local front velocities may subtract and cancel each other, which results in stationary spots with a slow fluid motion. Continuous development of the edge flow fronts may encounter the center flow front, leaving the stationary spot behind and finally generating unmovable air voids at the intersection of the flow fronts. The void formation by the racing effect is observed experimentally

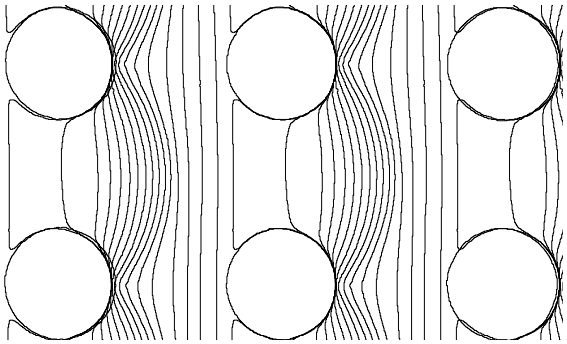

Fig. 12. Time-varying movement of the flow front passing through the solder bumps with a diameter of 50 μm, a pitch of 100 μm, and a gap height of 50 μm (Lee et al. [25]).

in Fig. 11. A transparent flip chip specimen (5 mm^2 × 5 mm^2, 50 μm gap height) was produced by etching the silicon part of a silicon-on-glass wafer in the form of a cylindrical bump (a diameter of 50 μm, a pitch of 100 μm). Fig. 11(a) illustrates the non-uniform flow fronts with different velocities at the early stage. The flow fronts converge, producing air voids because of the existence of a stationary region, as shown in Fig. 11(b). The voids that remain after the underfill process shown in Fig. 11(c) can be a crucial defect affecting the reliability of the flip chip package. An analytical condition of void formation for various underfill processes is difficult to define because of numerous factors affecting capillary flow, such as the rheological fluid properties, solder bump arrangement, surface condition of the flip chip, and liquid dispensing method, among others. Nevertheless, an underfill process with a tilted angle or a pressurized underfill process with a vacuumed air vent can be an alternative method to reduce the void formation and the total filling time [29, 30].

3.2 Interaction between the flow meniscus and the solder bumps

The dynamic interaction of the meniscus with the solder bumps is also crucial because it helps improve the analytical models or explain the physics of capillary flow through bumps and determine the methods of suppressing void formation by the racing effect. However, the experimental approach to this aspect remains unpopular. Lee et al. [25] measured the dynamics of the meniscus by microparticle image velocimetry and image processing techniques. Fig. 12 shows the time-varying flow front passing through the solder bumps. Given that the time separation between each flow front is the same, the narrow spacing between lines denotes low-speed movement, whereas the wide spacing denotes high-speed movement. In this figure, the meniscus moves fast once it attaches the solder bumps because of the attractive force of a stretched meniscus. However, before the meniscus detaches from the bump, its movement slows down because the direction of the capillary force changes negatively.

The phase-locked velocity fields at the instance of both the

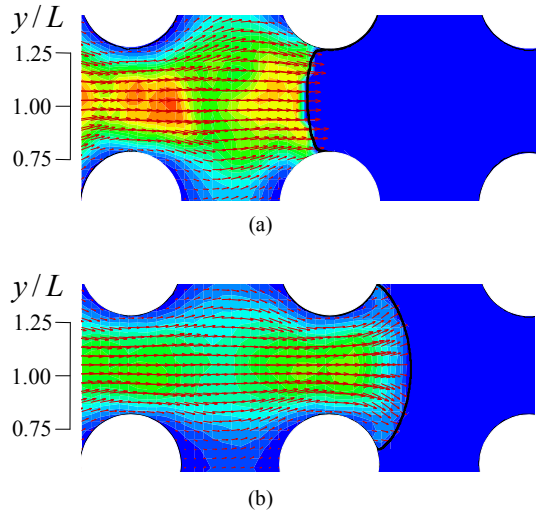

Fig. 13. Phase-locked velocity fields and contours of streamwise velocity measured at (a) the attaching process; (b) the detaching process (Lee et al. [25]).

attaching and detaching processes are plotted in Fig. 13. During the attaching process shown in Fig. 13(a), the velocity gradient on the meniscus is the highest, which induces additional normal stress on the meniscus surface. However, during the detaching process, the liquid velocity is extremely low except for the flow passage between bumps, as indicated in Fig. 13(b). The top view of the meniscus shows a concave or convex curvature because of the interaction with the solder bump, but its side view always shows a concave curvature. Thus, to analyze the detailed interaction, more sophisticated formulas for the capillary force in the three-dimensional shape have to be developed. The analyses of the movement of the inclined meniscus and its interaction with the solder bumps and velocity fields can still be challenged to clarify the physical phenomena of the stationary spot and void formation.

4. Summary and perspectives

The flip chip package has become increasingly thinner because of the demand for faster, smaller, and more flexible electronic devices. The underfill process in the flip chip package is a prerequisite to protect the electronic devices from thermal fatigue and drop impact. The recent achievements of the filling time models and the physical phenomena in the capillary underfill flows were reviewed in this study. As the solder bump density increases, the estimated filling time based on static capillary pressure becomes shorter than the measured filling time. This discrepancy results from the variation of the contact angle when the flow meniscus passes the bump surface. Therefore, the dynamic contact angle and its modeling should be considered to obtain a more accurate estimate of the capillary flow and its application. Apart from performance, the reliability of electronic devices is also significant in the industrial field. The presence of air voids after the underfill process indicates a serious packaging defect affecting reliability. The racing effect and stationary spots of the flow front lead to the formation of air voids. The higher the solder bump density, the greater is the probability of void formation. In such a case, the development of pressurized underfill technology with relevant air vents may be a viable alternative. To control the flow front uniformly for various bump arrangements, the interaction between the solder bumps and the flow meniscus should be investigated further from a microscopic perspective.

Acknowledgments

This study was supported by the Basic Science Research Program through the National Research Foundation of Korea funded by the Ministry of Education, Science, and Technology (2010-0009054).

References

[1] E. W. Washburn, The dynamics of capillary flow, *Phys. Rev.*, 17 (1921) 273-283.

[2] N. Ichikawa, K. Hosokawa and R. Maeda, Interface motion of capillary-driven flow in rectangular microchannel, *J. Colloid and Interface Sci.*, 280 (2004) 155-164.

[3] W. R. Jong, T. H. Kuo, S. W. Ho, H. H. Chiu and S. H. Peng, Flows in rectangular microchannels driven by capillary forces and gravity, *Int. Comm. Heat and Mass Transfer*, 34 (2007) 186-196.

[4] R. R. Tummala, *Fundamentals of Microsystems Packaging*, McGraw-Hill, Singapore, Singapore (2001).

[5] D. Suryanarayana, R. Hsiao, T. P. Gall and J. M. McCreary, Enhancement of flip-chip fatigue life by encapsulation, *IEEE Comp., Hybrids, and Manufacturing Technology*, 14 (1) (1991) 218-223.

[6] M. H. Gordon, G. Ni, W. F. Schmidt and R. P. Selvam, Capillary-driven underfill encapsulation process, *Advanced Packaging*, 8 (4) (1999) 34-37.

[7] V. S. Arpaci, *Conduction Heat Transfer*, Addison-Wesley Publishing Company, New York, USA (1966).

[8] L. Nguyen, C. Quentin, P. Fine, B. Cobb, S. Bayyuk, H. Yang and S. A. Bidstrup-Allen, Underfill of flip chip on laminates: simulation and validation, *IEEE Trans. Components and Packaging Technologies*, 22 (2) (1999) 168-176.

[9] G. Lehmann, A. Maria, P. -C. Lee and E. J. Cotts, Modeling the underfill flow process, *Proc. Technical Program, Conference on Surface Mount Technology*, San Jose, CA, USA (1997) 340-350.

[10] J. W. Wan, W. J. Zhang and D. J. Bergstrom, An analytical model for predicting the underfill flow characteristics in flip-chip encapsulation, *IEEE Trans. Advanced Packaging*, 28 (3) (2005) 481-487.

[11] K. Hosokawa, T. Fujii and I. Endo, Droplet-based nano/picoliter mixer using hydrophobic microcapillary vent, *Proc. IEEE MEMS*, Orlando, FL, USA (1999) 388-393.

[12] A. Gerlach, H. Lambach and D. Seidel, Propagation of adhesives in joints during capillary adhesive bonding of microcomponents, *Microsystems Technologies*, 6 (1999) 19-22.

[13] H. Schonhorn, H. L. Frisch and T. K. Kwei, Kinetics of wetting of surfaces by polymer melts, *J. Applied Phys*., 37 (13) (1966) 4967-4973.
[14] S. Newman, Kinetics of wetting of surfaces by polymers; capillary flow, *J. Colloid and Interface Sci.*, 26 (1968) 209-213.
[15] C. W. Macosko, *Rheology: Principles, Measurements, and Applications*, VCH Publishers, Inc., New York, USA (1994).
[16] R. B. Bird, W. E. Stewart and E. N. Lightfoot, *Transport Phenomena*, John Wiley & Sons, New York, USA (1960).
[17] J. W. Wan, *Analysis and modeling of underfill flow driven by capillary action in flip-chip packaging*, Ph.D Thesis at University of Saskatchewan, Saskatoon, Canada (2005).
[18] J. Wang, Underfill of flip chip on organic substrate: viscosity, surface tension, and contact angle, *Microelectronics Reliability*, 42 (2002) 293-299.
[19] W. B. Young and W. L. Yang, The effect of solder bump pitch on the underfill flow, *IEEE Trans. Advanced Packaging*, 25 (4) (2002) 537-542.
[20] W. B. Young, Capillary impregnation into cylinder banks, *J. Colloid and Interface Sci*., 273 (2004) 576-580.
[21] B. R. Gebart, Permeability of unidirectional reinforcements for RTM, *J. Composite Mater*., 26 (8) (1992) 1100-1133.
[22] S. Han and K. K. Wang, Analysis of the flow of encapsulant during underfill encapsulation of flip-chips, *IEEE Trans. Components, Packaging, and Manufacturing Technology-Part B*, 20 (4) (1997) 424-433.
[23] J. W. Wan, W. J. Zhang and D. J. Bergstrom, Experimental verification of models for underfill flow driven by capillary forces in flip-chip packaging, *Microelectronics Reliability*, 48 (2008) 425-430.
[24] Y. B. Kim, J. Sung and M. H. Lee, Micro-PIV measurements of capillary underfill flows and effect of bump pitch on filling process, *J. Visualization*, 14 (2011) 237-248.
[25] S. H. Lee, J. Sung and S. E. Kim, Dynamic flow measurements of capillary underfill through a bump array in flip chip package. *Microelectronics Reliability*, 50 (2010) 2078-2083.
[26] P. Fine, B. Cobb and L. Nguyen, Flip-chip underfill flow characteristics and prediction, *IEEE Trans. Components and Packaging Technologies*, 23(3) (2000) 420-427.
[27] J. W. Wan, W. J. Zhang and D. J. Bergstrom, Numerical modeling for the underfill flow in flip-chip packaging, *IEEE Trans. Components and Packaging Technologies*, 32 (2009) 227-234.
[28] T. Hashimoto, T. Shin-ichiro, K. Morinishi and N. Satofuka, Numerical simulation of conventional capillary flow and no-flow underfill in flip-chip packaging, *Computers and Fluids*, 37 (2008) 520-523.
[29] J. Wang, Flow time measurements for underfills in flip-chip packaging, *IEEE Trans. Components and Packaging Technologies*, 28 (2005) 366-370.
[30] S. Han and K. K. Wang, Study on the pressurized underfill encapsulation of flip chips, *IEEE Trans. Components, Packaging, and Manufacturing Technology-Part B*, 20 (4) (1997) 434-442.

Young Bae Kim He obtained his BS degree in Environmental Engineering from Yonsei University in 2007. Since then, he has been a graduate student of Energy and Environmental Engineering at Seoul National University of Science and Technology.

Jaeyong Sung He received his BS degree in Mechanical Engineering from the Seoul National University in 1994. He subsequently obtained MS and Ph.D degrees from the School of Mechanical and Aerospace Engineering at Seoul National University in 1996 and 2001. Since 2004, he has been a professor in the Department of Mechanical and Automotive Engineering at Seoul National University of Science and Technology.